

Separating polarized cosmological and galactic emissions for CMB B-mode polarization experiments

Federico Stivoli¹, Carlo Baccigalupi^{1,2,3,4}, Davide Maino⁵, Radek Stompor^{6,7,8}

¹ *SISSA/ISAS, Astrophysics Sector, Via Beirut, 4, I-34014 Trieste, Italy*

² *Institut für Theoretische Astrophysik, Universität Heidelberg, Albert-berle-Strasse 2, D-69120 Heidelberg, Germany*

³ *INFN, Sezione di Trieste, Via Valerio 2, I-34014 Trieste, Italy*

⁴ *Physics Division, Lawrence Berkeley National Laboratory, 1 Cyclotron Road, Berkeley, CA 94720, USA*

⁵ *Dipartimento di Fisica, Università di Milano, Via Celoria 16, I-20133, Milano, Italy*

⁶ *Computational Research Division, Lawrence Berkeley National Laboratory, 1 Cyclotron Road, Berkeley, CA 94720, USA*

⁷ *Space Sciences Laboratory, University of California, Berkeley, CA 94720, USA*

⁸ *Laboratoire Astroparticule et Cosmologie, Université Paris-7, Paris, France*

8 November 2018

ABSTRACT

The detection and characterization of the B mode of Cosmic Microwave Background (CMB) polarization anisotropies will not be possible without a high precision removal of the foreground contamination present in the microwave band. In this work we study the relevance of the component separation technique based on the Independent Component Analysis (ICA) for this purpose and investigate its performance in the context of a limited sky coverage observation and from the viewpoint of our ability to differentiate between cosmological models with different primordial B-mode content.

We focus on the low Galactic emission sky patch centered at 40 degrees in right ascension and -45 in declination, corresponding to the target of several operating and planned CMB experiments and which, in many respects, adequately represents a typical “clean” high latitude sky. We consider two fiducial observations, one operating at low (40, 90 GHz) and one at high (150, 350 GHz) frequencies and thus dominated by the synchrotron and thermal dust emission, respectively. We use foreground templates simulated in accordance with the existing observations in the radio and infrared bands, as well as the Wilkinson Microwave Anisotropy Probe (WMAP) and Archeops data and model the CMB emission adopting the current best fit cosmological model, with an amplitude of primordial gravitational waves either set to zero or 10%. We use a parallel version of the FASTICA code to explore a substantial parameter space including Gaussian pixel noise level, observed sky area and the amplitude of the foreground emission and employ large Monte Carlo simulations to quantify errors and biases pertinent to the reconstruction for different choices of the parameter values. We identify a large subspace of the parameter space for which the quality of the CMB reconstruction is excellent, i.e., where the errors and biases introduced by the separation are found to be comparable or lower than the uncertainty due to the cosmic variance and instrumental noise. For both the cosmological models, with and without the primordial gravitational waves, we find that FASTICA performs extremely well even in the cases when the B mode CMB signal is up to a few times weaker than the foreground contamination and the noise amplitude is comparable with the total CMB polarized emission. In addition we discuss limiting cases of the noise and foreground amplitudes, for which the ICA approach fails.

Although our conclusions are limited by the absence of systematics in the simulated data, these results indicate that these component separation techniques could play a

crucial role in the forthcoming experiments aiming at the detection of B modes in the CMB polarization.

Key words: methods – data analysis – techniques: image processing – cosmic microwave background.

1 INTRODUCTION

The main target of the planned probes for measuring the polarized component of the Cosmic Microwave Background (CMB) radiation is represented by the B modes, also known as “curl” component (Zaldarriaga, Seljak 1997; Kamionkowski et al. 1997). The CMB B mode signal is known to be generated by primordial gravitational waves and the weak lensing due to structures forming in the Universe (Zaldarriaga, Seljak 1998), and thus contains unique information about the early Universe, and, potentially, physics of high energies.

The B signal in the CMB polarization is more than one order of magnitude smaller than the “gradient” mode (E) coming from all kinds of cosmological perturbations, and about two orders of magnitude lower if compared with the total intensity anisotropies (T). The CMB E mode and the TE cross-correlation, have been detected by the WMAP satellite (Page et al. 2006) as well as instruments operating on the ground (Kovac et al. 2002; Readhead et al. 2004) and from balloons (Montroy et al. 2005). No glimpse of the B has been seen so far and it is apparent that its detection will represent an experimental and data analysis challenge in terms of control and treatment of systematics and instrumental noise needed to attain the required precision. An additional important limiting factor for these experiments is related to foreground emissions. In the frequency range going from 70 to 150 GHz the diffuse Galactic emission is known to be sub-dominant with respect to the total intensity CMB signal at medium and high Galactic latitudes. The knowledge of polarized foregrounds has been given a boost by the observations by Archeops (Benoit et al. 2004) and most importantly the WMAP three year data (Page et al. 2006). However, the foreground polarized pattern, especially at high Galactic latitudes, remains quite unknown; these new findings confirm the earlier guess that the weakness of the cosmological B signal makes the foreground contamination, at least potentially and, more likely, certainly very important for the recovery of this component everywhere in the sky and at any frequency (Baccigalupi 2003).

In this context, it is crucial to develop reliable data analysis techniques and tools which are capable of cleaning the CMB emission from the foreground contamination, prior to assessing what is the minimum level of amplitude in the B modes which is detectable in presence of foregrounds. Although preliminary investigations concerning the minimum detectable level of primordial tensors exist (Tucci et al. 2005), no satisfactory answer has been given yet, essentially because of the foreground uncertainties (Baccigalupi 2003). Algorithms aiming at the reduction of the foreground contamination in CMB observations belong to the category of the component separation techniques. Those are designed to use multi-frequency information to separate emissions observed in the same frequency bands but produced by different physical processes. If robust prior knowledges are available about the signal to recover, the maximum entropy method (Hobson et al. 1998; Stolyarov et al. 2002) or Wiener filtering (Tegmark, Efstathiou 1996; Bouchet et al. 1999) may be implemented. On the other hand, in the case of CMB polarization, the polarized foregrounds are likely to be greatly uncertain even at the time when the analysis of the future CMB data will be already on-going, and thus alternative approaches, not relying on such priors, may be required. The class of “blind” component separation techniques exploits the statistical independence of the sky signals to be separated, a natural expectation for the CMB and Galactic emissions.

Among the techniques in this category, the Independent Component Analysis (ICA) (Amari, Chichocki 1998; Hyvärinen 1999) has been considered in several works concerning component separation. It was first exploited as a neural network, i.e. capable of self-adjusting on time varying data streams (Baccigalupi et al. 2000), and then developed in a form of a numerically fast algorithm and a code, FASTICA, capable of operating on a data set as nominally anticipated from the Planck experiment (Maino et al. 2002). The latter approach has been successfully tested on the real data from COBE/DMR (Maino et al. 2003), recovering the main CMB results of that experiments, e.g., with respect to the amplitude and power spectrum of the cosmological perturbations on large scales, and also on the data of the BEAST experiment (Donzelli et al. 2005). A flexible version of the ICA algorithm, capable to exploit available priors, has been proposed (Delabrouille et al. 2003). Recently, the FASTICA algorithm was applied to simulated Planck data in polarization on all sky (Baccigalupi et al. 2004).

In the forthcoming years, the detection of the B modes will be attempted by balloon and ground based experiments, targeting sky regions where the foreground emission in total intensity is known to be low. One of those regions is centered on the position ($40^\circ, -45^\circ$) in right ascension and declination. This region has been observed by BOOMERanG 2K (Montroy et al. 2005), and is the target of the EBEx (Oxley et al. 2004), QUAD (Bowden et al. 2004) and QUIET experiments¹. However, a low amplitude of the foreground emission in total intensity does not ensure that on a level of the anticipated cosmological

¹ For a list of the operating and planned CMB polarization experiments see lambda.gsfc.nasa.gov.

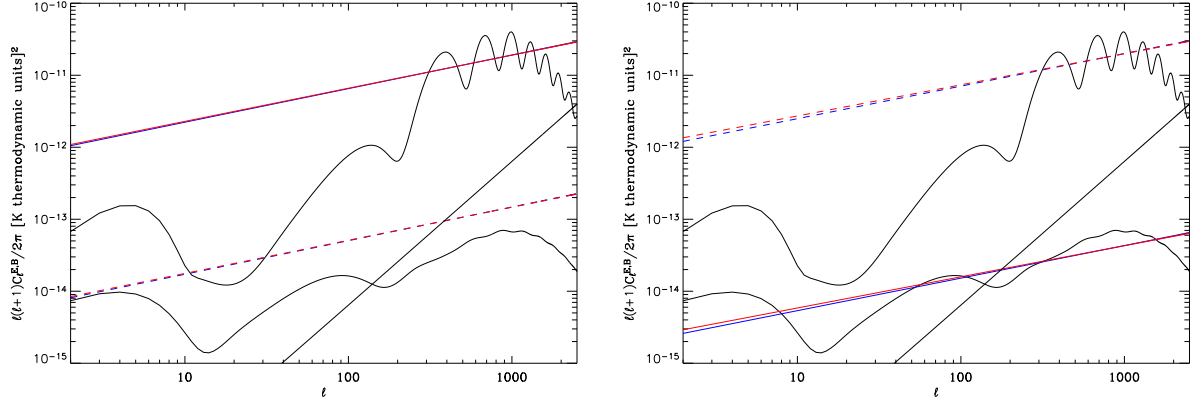


Figure 1. Power spectra of the different polarized sky signals relevant to the microwave observations. The almost flat straight lines represent the foreground contamination obtained by cutting out the Galactic plane up to $|b| = 50^\circ$, and fitting those with a power law; the steep straight lines raising as ℓ^2 represent the instrumental noise assumed in this work. The left and right panels show the predictions for the 40, 90 GHz and 150, 350 GHz frequency bands, respectively. The solid lines represent a lower frequency, while the dashed ones a higher one. These signals are plotted against the full sky CMB power spectra of anisotropies in thermodynamical units for E and B as assumed in this work (oscillating solid curves).

B -mode signal the polarized foregrounds can *a priori* be considered irrelevant. Therefore in this work we test the FASTICA performance in the reconstruction of the CMB polarized emission on that region of the sky, focusing on the recovery of B modes. Our work represents an exploratory study, not specialized to describe any particular operating or planned experiment, nor to quantify what is the minimum level of B modes detectable in presence of foregrounds. Our aim is rather to determine if the blind component separation techniques have the capability to recover the B modes of the CMB, which are on the level as predicted in the current best fit cosmological models and are observed on a limited patch of the sky in the presence of a substantial foreground contamination as estimated on the basis of the current models of the Galactic emission. In section 2 we describe how the background and foreground signals are simulated, while in section 3 we describe how the angular power of the CMB polarization anisotropies on a limited portion of the sky is computed. In section 4 we present a parallel version of the FASTICA algorithm (LIGHTICA) operating on polarization data and apply it to the simulated sky signal realization to evaluate biases and stability of the B mode reconstruction against variations in the background and noise realizations, noise and foreground fluctuation amplitude and extension of the sky area considered. In section 5 we discuss the implications of our results for what concerns the recovery of the primordial tensor to scalar ratio. Finally, in section 6 we discuss and summarize our results.

2 SIMULATED MAPS

The CMB emission is simulated accordingly to the cosmological concordance model (Spergel et al. 2003). The Hubble constant is $H_0 = 72$ km/s/Mpc, the overall geometry is flat, with a critical density made of baryons (4.4%), Cold Dark Matter (CDM) (22.6%), and the cosmological constant (73%). The radiation component consists of photons and three massless neutrino species. The optical depth to the last scattering surface is fixed at $\tau = 0.11$. The perturbations are Gaussian, with a primordial power spectrum characterized by a spectral index of scalar perturbations $n_s = 0.96$. Unless otherwise specified, the primordial gravity wave contribution is set to 10% of the scalar perturbation amplitude, with a spectral index fixed accordingly to the single field inflationary model, $n_t = -n_s/6.8$. When explicitly specified, we also consider the case in which no gravity waves are present. We include the contribution due to lensing in the power spectrum, which is responsible for substantial part of the power in the B modes of the CMB polarization anisotropies. The statistics of this component is non-Gaussian because of the correlation of different scales induced by lensing itself (Smith et al. 2004), and that could be exploited to separate it from the primordial B -mode signal (Seljak, Hirata 2004). On the other hand, as we show in the next Section, on a limited patch of the sky considered here, the angular power spectrum for B is substantially affected by the leakage coming from the E modes and which thus obey the Gaussian statistics of the primordial fluctuations. Given this and the fact that, in the following we consider only 2-point statistics, we assume that the entire B -mode signal is Gaussian. The power spectrum of CMB anisotropies is calculated using CMBFAST (Seljak, Zaldarriaga 1996) while the sky realizations have been obtained using the HEALPix package², assuming the Gaussian statistics. In antenna units, the CMB fluctuations at a frequency ν are

² <http://www.eso.org/science/healpix/>

obtained by the thermodynamical one by multiplying by the factor $x^2 \exp(x)/[\exp(x) - 1]^2$, where $x = h\nu/kT_{\text{CMB}}$, h and k are the Planck and the Boltzmann constant, respectively, while $T_{\text{CMB}} = 2.726$ K is the CMB thermodynamical units.

The polarized synchrotron emission has been simulated accordingly to two distinct recipes. Both of them derived a template for the polarization angle θ by exploiting the observations in the radio band: these measures indicate a rather high fluctuation level interpreted as the effect of the small scale structure of the Galactic magnetic field (Uyaniker et al. 1999; Duncan et al. 1999), scaling as $C_l^\theta \sim l^{-2}$ on degree and sub-degree angular scale, up to the arcminute (Tucci et al. 2002), consistently also with recent observations at medium Galactic latitudes (Carretti et al. 2005). It is worth noting here that WMAP three year analysis shows an evidence for a shallower slope in the polarization angle pattern, at least on large angular scales and intermediate Galactic latitudes (Page et al. 2006). The template for the polarization angle was obtained by adopting the form above for C_l^θ , and assuming Gaussian distribution. The distinction between the two recipes is in the model assumed for the polarized intensity. In Baccigalupi et al. (2001), it was derived directly from the observations in the radio band including the existing data on large angular scale (Brouw, Spoelstra 1976). On the other hand, Giardino et al. (2002) exploited the all sky template of synchrotron in total intensity at 408 MHz (Haslam et al. 1982), assuming a theoretically synchrotron polarization fraction of about 75%; since the latter template has a resolution of about one degree or less, they extrapolated the power to the smaller scales by exploiting the total intensity observations in the radio band (Uyaniker et al. 1999; Duncan et al. 1999). The recipe adopted by Giardino et al. (2002) yields a stronger signal, and is what we take in this work as the polarized synchrotron template. In antenna units, the frequency scaling of the synchrotron is related to the energy distribution of electrons, exhibiting a steep power law as ν^{-3} , according to the observations of WMAP at intermediate and high Galactic latitude (Bennett et al. 2003) and as adopted in this paper.

The polarized emission from the diffuse thermal dust has been detected for the first time in the Archeops data (Benoit et al. 2004), indicating a 5% polarization fraction with respect to the total intensity emission, which is very well known at $100\mu\text{m}$ and can be extrapolated at microwave frequencies fitting for the emissivity and temperature of two thermal components (Finkbeiner et al. 1999). In this work, we adopt the model 8 of Finkbeiner et al. (1999), where dust emissivity and temperatures do not vary across the sky. The dust polarization fraction reported by WMAP three years is also consistent with a few percent. The pattern of the polarization angle is much more uncertain, and due to the magnetized dust grains which get locally aligned along the Galactic magnetic field (Prunet et al. 1998; Jones et al. 1995). Since the geometry and composition of the dust grains is still very uncertain, the simplest assumption is that the Galactic magnetic field is 100% efficient in imprinting the polarization angle pattern to the synchrotron and dust emission (Baccigalupi 2003).

Although the knowledge of the polarized foregrounds summarized above may be exploited to build their all sky models, the resulting templates, though useful are still affected by a substantial uncertainty, and hence need to be utilized with a caution. For synchrotron, the uncertainties are mainly due to a poor resolution of the available total intensity template (Haslam et al. 1982), which corresponds to an angular scale of a degree or larger, and, which in addition is polluted by HII regions at low Galactic latitudes (Baccigalupi et al. 2001). Moreover, the polarized signal is observed in the radio band only, and at low Galactic latitudes, where a substantial Faraday depolarization may significantly affect the true synchrotron pattern. Indeed, as we already mentioned, WMAP three years reports evidence of a shallower slope in the power spectrum of polarized fluctuations of diffuse foregrounds, although that claim is limited essentially by sensitivity to large angular scales and intermediate Galactic latitudes (Page et al. 2006). The dust model is much better known in total intensity, but the polarization fraction has again been measured at low Galactic latitudes only, and on large angular scales. Moreover the dust polarization angle distribution suffers the same uncertainty as in the synchrotron case, as in the modeling the two are commonly assumed to be identical.

Despite of these missing pieces, this represents the present state of the art in the simulation of the polarized Galactic foreground emission, at least on scales and Galactic latitudes still hidden to WMAP. The forecasted contamination is particularly challenging for the B mode CMB measurements; indeed, as this signal, arises only from the primordial gravitational waves and the weak lensing effect of the E polarization (Zaldarriaga, Seljak 1997, 1998), it is about one order of magnitude smaller than the E component. On the other hand, the Galactic foregrounds are expected to have almost the same power in the two modes (Zaldarriaga 2001), as WMAP three year results confirmed remarkably.

In figure 1 we show the contamination to the all sky CMB E and B spectra from the foreground emission corresponding to the synchrotron and dust diffuse Galactic signal after cutting out the Galactic plane up to $|b| = 50^\circ$, roughly corresponding to the latitudes considered in this work, as we explain below. The foreground power has been evaluated by fitting the actual sky signal with a power law, $C_l = \alpha l^\beta$. As it is evident, the models of the foreground emission indicate that the contamination to the B modes of the CMB is relevant in all cases. The lines raising as l^2 represent the levels of instrumental noise which we consider in this work, as explained in detail in section 4.

In this work we study the performance of the ICA technique on diffuse signals in polarization, and we do not consider the effect of extra-Galactic point sources, although this point is certainly crucial in realistic conditions; indeed the current models (Tucci et al. 2004) suggest that the residual power from unresolved point sources could be comparable to the level of noise we treat here, at least at the lowest frequency we considered, and although the results we show next are quite stable against the noise amplitude, this point warrants a further investigation in forthcoming works. We come back to this point in the

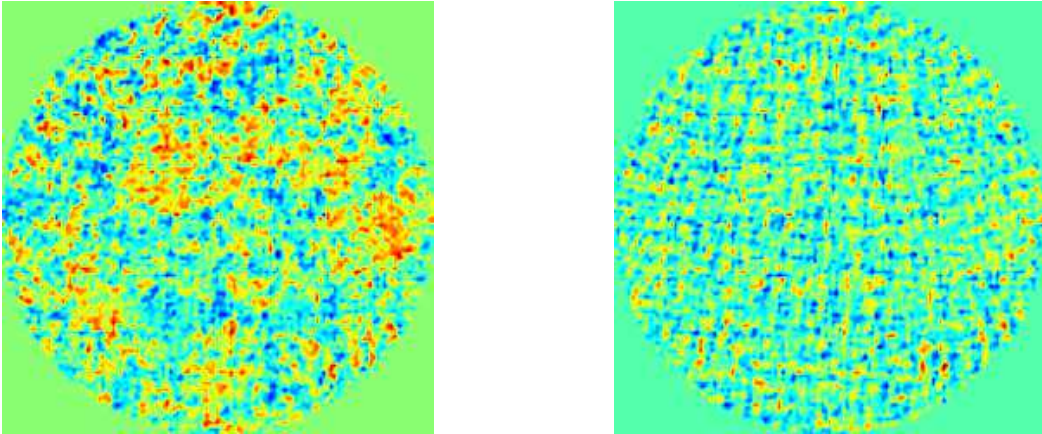


Figure 2. The total (CMB plus foregrounds) Q Stokes parameter emission in the sky area considered in this work, at 40 (left) and 90 GHz (right). At 90 GHz the signal appears dominated by the CMB signal, while the synchrotron contamination is evident at 40 GHz.

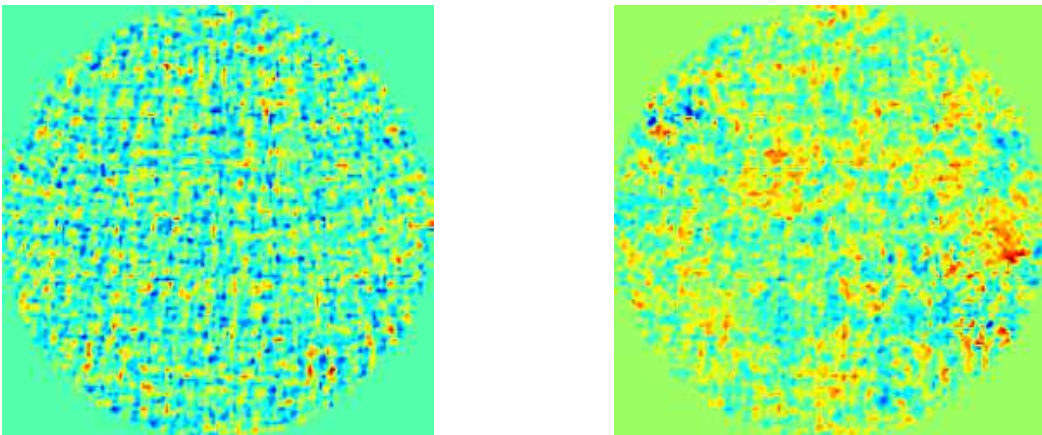


Figure 3. The total Q Stokes parameter emission in the sky area considered in this work, at 150 (left) and 350 GHz (right). At 150 GHz the signal appears dominated by the CMB emission, while the dust emission dominates at 350 GHz.

conclusions.

We shall consider a circular sky patch with a radius $\theta_C = 10^\circ$ and 20° , corresponding to about 0.76% and 3.04% of the entire sky, respectively. The center in Galactic coordinates is at $l = 260^\circ$, $b = -62^\circ$, within the region considered by different experiments (Montroy et al. 2005; Bowden et al. 2004; Oxley et al. 2004). We take two frequency combinations, 40, 90 GHz, and 150, 350 GHz, where the dominant foreground emission is represented by the synchrotron and the thermal dust, respectively. The sky emission at the various frequencies, corresponding to the Q Stokes parameter, is shown in figures 2 & 3. At 90 and 150 GHz the CMB signal appears relatively free of foreground contamination, while at 40 and 350 GHz the foregrounds dominate. In Section 4 we describe more quantitatively the foreground CMB contamination by means of the angular power spectrum, defined formally in the next Section when a limited part of the sky is considered.

3 POLARIZATION PSEUDO POWER SPECTRA

In this work we apply the ICA component separation technique on a portion of the sky. We will quantify the quality of the reconstruction with help of the angular (pseudo-)power spectra, which are relevant and straightforwardly calculable for the limited sky observations as considered here. In a computation of the polarized, E and B (pseudo-)power spectra on a finite portion of the sky a transfer of power between the E and B modes occurs (see Chon et al. 2004, and references therein). Since the B modes are sub-dominant, the leakage of the E -mode power alters their spectrum more substantially and consequently needs to be explicitly considered in the presented analysis. In this paper we will denote the pseudo power spectra of E and B as \tilde{C}_l^E and \tilde{C}_l^B , respectively, while the symbols without a tilde will correspond to their full-sky versions. Hereafter we compute the power spectra using a recipe adopted from Hansen et al. (2002). Consequently, we introduce a window function, $G(\theta, \phi)$,

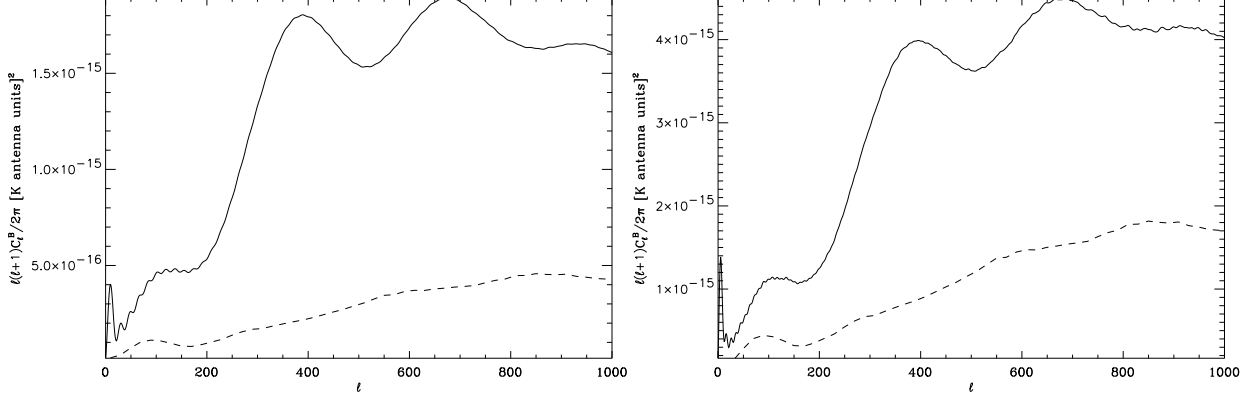


Figure 4. Pseudo power spectra for the B modes, in the case of a circular top hat cut of $\theta_C = 10^\circ$ (left panel, solid line) and $\theta_C = 20^\circ$ (right panel, solid line). The dashed lines in both panels represent the full sky C_l^B normalized to the patch area fractions. The contamination due to the E mode is evident.

(Gabor 1946) which is applied to the data prior to a computation of the spherical harmonic transforms on a portion of the sphere and a calculation of the pseudo-power spectra. The leakage between the polarization modes may be written as

$$\tilde{C}_l^E = \sum_{l'} C_{l'}^E K_2(l, l') + \sum_{l'} C_{l'}^B K_{-2}(l, l'), \quad (1)$$

$$\tilde{C}_l^B = \sum_{l'} C_{l'}^B K_2(l, l') + \sum_{l'} C_{l'}^E K_{-2}(l, l'), \quad (2)$$

where C_l^E and C_l^B are the polarization full-sky power spectra (Zaldarriaga, Seljak 1997), while the kernels $K_2(l, l')$ and $K_{-2}(l, l')$ depend on the form and the size of the cut, described by a generic function $G(\theta, \phi)$ which is zero in the sky regions which are not considered. The explicit expressions for the kernels are:

$$K_{\pm 2}(l, l') = \sum_{l''} g_{l''}^2 \frac{(2l' + 1)(2l'' + 1)}{32\pi^2} W^2(l, l', l'') (1 \pm (-1)^{l+l''}). \quad (3)$$

Here g_l are found by the inverse Legendre transform of the Gabor window $G(\theta, \phi)$ and the Wigner symbols W are defined as:

$$W(l, l', l'') = \begin{pmatrix} l & l' & l'' \\ -2 & 2 & 0 \end{pmatrix}. \quad (4)$$

We exploited these formulae for circular cut sky area of different size with top hat shape:

$$G(\theta) = \begin{cases} 1, & \theta \leq \theta_C, \\ 0, & \theta > \theta_C. \end{cases} \quad (5)$$

As one can see from equations (1) and (2), the sky cut mixes the polarization E and B modes, as quantified by the $K_{-2}(l, l')$ kernel. Obviously, the mixing gets reduced as the size of the window is increased. Since the cosmological fluctuations are dominated by the scalar contribution in the cosmological concordance model (Spergel et al. 2003), even if the diagonal of the kernel $K_2(l, l')$ is one order of magnitude larger than the diagonal of $K_{-2}(l, l')$, we expect the E mode to contaminate substantially the B signal even for large regions of the sky, while on the other hand $\tilde{C}_l^E \simeq C_l^E$.

In Fig.4 we show the pseudo power spectrum of the B mode, \tilde{C}_l^B , as defined in (2) for a top hat window with $\theta_C = 10^\circ$ and 20° . In the latter case, the leakage from the E modes is slightly weaker. (Hereafter, we limit our analysis to a range of l -modes ≤ 1000 in order to speed up the calculation of the pseudo- C_l s.) For comparison the dashed lines show the full sky B mode power spectra (with power normalized on the patch). As we see, the shapes of the two spectra are substantially different and the E mode contamination is relevant for the pseudo- C_l^B .

4 COMPONENT SEPARATION

In this Section we present a first application of the LIGHTICA code, based on FASTICA, optimized for parallel runs and operating on polarization data. We first describe the basic features of the algorithm, then show its performance on our simulated data. We do not report here all the details of the FASTICA technique, as they may be found in earlier works, concerning total intensity (Maino et al. 2002) and polarization (Baccigalupi et al. 2004). As described above, we consider here

two frequency combinations, 40 and 90 GHz, 150 and 350 GHz, where the CMB is contaminated by synchrotron and dust diffuse polarized emission, respectively. The CMB is added to the foregrounds at the different frequencies in Q and U , expressed in Kelvin antenna units. We adopt a spatial resolution of about $3.5'$ arcminutes, corresponding to $n_{side} = 1024$ resolution parameter in the HEALPix pixelization scheme. Before processing, all the maps have been smoothed with a Gaussian, circular beam with full width half maximum (FWHM) equal to 10 arcminutes; moreover, a Gaussian and uniformly distributed noise is added, with amplitude specified below. As we stress in the following, the high resolution is a crucial requirement for a successful application of the ICA techniques, as they do not rely on any other priors than the statistical independence of the signal to reconstruct, and need a large number of realizations to converge to the solution. The spatial resolution considered here is close to the values anticipated for the forthcoming experiments (Montroy et al. 2005; Bowden et al. 2004; Oxley et al. 2004).

In all the cases we show, a single separation run (not including the construction of the simulated sky) takes about 5 seconds on a workstation with 1.5 Gb RAM and 2.4 GHz Pentium IV processor.

4.1 LIGHTICA: an MPI parallel implementation of the FASTICA component separation in polarization

The core of the ICA technique is based on a maximization of an approximation of the neg-entropy, which measures the distance of a mixture of signals from a Gaussian distribution (Amari, Chichocki 1998; Hyvärinen 1999). The hypothesis are that the mixture contains at most one Gaussian component and that all of them obey different probability distributions and frequency scalings; if this is verified, it is possible to demonstrate that asymptotically in the number of realizations (pixels in our case), the local maxima of the neg-entropy correspond to the components present into the mixture. The excellent performance obtained so far on simulated CMB data is due mainly to two features: the good detail in the maps, reaching the arcminute scale, as well as the high level of independence between the background CMB and the foreground emissions (Maino et al. 2002; Baccigalupi et al. 2004). As reported in the latter reference the FASTICA technique can be, and has been, applied to sky maps of Q and U Stokes parameters, and which subsequently can be used to derive constraints on the E and B power spectra.

Given those promising results, and aiming at the application of the method to real polarization data, it is important to develop a framework for evaluating the errors of the separation as well as for studying its performance for a broad set of values of basic parameters characterizing any data set. The relevant parameters in this case include instrumental noise, CMB realizations, foreground properties, area covered by a given experiment and others. Along with pure theoretical consideration, these two issues may be addressed with the help of suitable Monte Carlo simulations. Due to the remarkable speed of a single ICA component separation run, this technique is well suited for straightforward parallelization with only a memory management and I/O issues calling for more elaborate solutions. In the LIGHTICA code, the main ICA routine, operating on arrays of numbers, is called by each processor processing its own version of the sky (or part thereof). The code consists in a main driver performing the following steps. A number of CMB realizations is pre-computed and a set of external parameters determines the case under study, namely set of frequencies, foreground fluctuation amplitude, noise amplitude, etc. For each CPU, first, the driver generates random numbers representing random noise in the data. Then it calls a separate routine co-adding the different sky components as defined by the external run parameters. The sky components are represented in the HEALPix format and the co-addition is done separately for the Q and U Stokes parameters. Let \mathbf{x}^Q and \mathbf{x}^U be the multi-frequency data, where \mathbf{x} is labeled by two indices, numbering frequencies (rows) and pixels (columns). The algorithm assumes that the components scale rigidly with frequency, which means that each of them can be represented by a product of two functions each depending either on a frequency or a direction (i.e., a pixel). We define a spatial pattern for them, which we denote with either \mathbf{s}^Q or \mathbf{s}^U and express the inputs $\mathbf{x}^{Q,U}$ as

$$\mathbf{x}^{Q,U} = \mathbf{A}^{Q,U} \mathbf{s}^{Q,U} + \mathbf{n}^{Q,U}, \quad (6)$$

Here the matrices $\mathbf{A}^{Q,U}$ scale the spatial patterns of $\mathbf{s}^{Q,U}$ to the input frequencies; the instrumental noises $\mathbf{n}^{Q,U}$ have same dimensions as \mathbf{x} . Note that equation (6) implies that all the frequencies has the same spatial resolution, which is not the case in real observations and is one of the limitations of the ICA technique in pixel space, effectively forcing the analysis to be performed at the lowest resolution of a given experiment.

The constructed skies are given as inputs to the main ICA core routine performing the separation. The maximization of the neg-entropy computes two separation matrices, \mathbf{W}^Q and \mathbf{W}^U , and produces a copy of the independent components present in the data:

$$\mathbf{y}^Q = \mathbf{W}^Q \mathbf{x}^Q, \quad \mathbf{y}^U = \mathbf{W}^U \mathbf{x}^U. \quad (7)$$

More details on the way the separation matrix for FASTICA is estimated are given in previous works (Maino et al. 2002; Baccigalupi et al. 2004), together with a recipe how to recover the frequency scaling of the signals $\mathbf{s}^{Q,U}$. The resulting \mathbf{y}^Q and \mathbf{y}^U can be combined together to get the E and B modes for each reconstructed component. Note that the noise correlation matrix can be taken into account in the separation process; this is done simply by subtracting the noise correlation matrix

from the one of the total signal before entering into the core of the algorithm (Hyvärinen 1999); for an uniform and Gaussian distributed noise, its correlation matrix is null except on the diagonal, containing the noise variances at the frequencies considered. Of course even in the case of a perfect separation, the derived outputs will be noisy as implied by equations (6,7). Consequently, whenever the separation matrices, $\mathbf{W}^{Q,U}$, are well-constrained by data, the dominant contribution to the noise level is adequately approximated by,

$$\mathbf{n}_y^{Q,U} = \mathbf{W}^{Q,U} \mathbf{n}^{Q,U}. \quad (8)$$

This means that, if the noises for different channels are uncorrelated and Gaussian, and denoted as σ_{ν_j} the input noise root mean square (*rms*) at frequency ν_j , the noise *rms* on the i -th output is

$$\sigma_{y_i}^{Q,U} = \sqrt{\sum_j |W_{ij}^{Q,U}|^2 |\sigma_{\nu_j}^{Q,U}|^2}. \quad (9)$$

For full sky signals, the noise contamination to the angular power spectrum is $C_{l,n_i}^{Q,U} = 4\pi(\sigma_{y_i}^{Q,U})^2/N$, where N is the number of pixels. The Gaussianity and uniformity assumptions make it easy to calculate the noise level on E and B modes, since they contribute at the same level: $C_{l,n_i}^E = C_{l,n_i}^B = (C_{l,n_i}^Q + C_{l,n_i}^U)/2$. The latter quantities represent the average noise power, which can be simply subtracted from the output power spectra by virtue of the lack of correlation between noise and signal. The remaining uncertainty comes from noise realization, which at 1σ and on the whole sky is: $\Delta C_{l,n(i)}^{E,B} = \sqrt{2/(2l+1)} C_{l,n(i)}^{E,B}$. The final step consists in the output of the results. Those may be in the form of maps or power spectra, computed simply with the HEALPix routines. The code also outputs the separation matrix and its inverse as computed by each processor.

The overall structure of the LIGHTICA is rather flexible; in particular, the header dealing with different variables may be easily changed and specialized for studying a particular degree of freedom. It is also quite extensible and, for example, the OPENMP HEALPix routines can be easily incorporated if a further speed-up of the power spectrum computation is desired. In the following we present the first applications of LIGHTICA. We choose and analyze a suitable reference simulated dataset, and then we study the stability of the results against variation of some among the most relevant degrees of freedom of the simulated dataset. In each case, the separation quality is quantified by the ICA induced bias and additional uncertainty of the recovered CMB spectra as evaluated in each Monte Carlo series.

4.2 B modes reconstruction and error estimation

The sky signals in the patch considered are processed by the LIGHTICA code, and the outputs, in E and B , are shown in figures 5, 6, and 7, 8, respectively. Those are plotted at 40 and 150 GHz in antenna units, as the code outputs are at the lowest frequency by default. In each panel, the two dotted curves correspond to the theoretical pseudo- $C_l^{E,B}$ of the CMB signal, $\pm 1\sigma$ where σ represents the cosmic variance on our patch of the sky: that is specified by a fraction f_{sky} and binned over $\Delta l = 50$ multipoles (Tegmark 1997), and is given by

$$\Delta \tilde{C}_l^{E,B} = \sqrt{\frac{2}{(2l+1)\Delta l f_{sky}}} (\tilde{C}_l^{E,B} + \tilde{C}_{n,l}^{E,B}), \quad (10)$$

where $\tilde{C}_{n,l}^{E,B}$ are the contribution of the noise. We assume a Gaussian and uniformly distributed noise over the analyzed region, with *rms* equal to a half of that of the CMB Stokes parameter Q or U on a single pixel, at each frequency. The noise amplitude is not related to any particular experiment, and was chosen as a starting point for the analysis performed in the next sub-section, where the noise amplitude is varied. Note that, in the case of full sky coverage, the chosen noise amplitude is shown in figure 1.

The symbols in the figures represent the signal recovered by the LIGHTICA separation process averaged over the 100 MC simulations of the CMB and noise, while the error bars show, a 1σ uncertainty derived from the simulations. Thus, they represent the error in the separation process, given the foreground templates assumed in this work. At the bottom of each figure, we also plot the average and standard deviation of the residuals, obtained by subtracting the input from the output pseudo-power spectra for each realization. The averages provide a measure of biases of the reconstruction on each realization, while the error bars estimate the extra dispersion introduced due to the separation process.

The first feature to be noted is that the separation is clearly successful, for E and B as well. Note that the B-mode pseudo-power spectra are generally comparable or lower than the foreground and noise contamination, as we show explicitly in the next sub-section. As we stressed above, the ICA technique looks for the independent components into the data, assuming rigid and different frequency scaling and a different statistics for all of them, with no other prior; the fact that this procedure is able to extract with such a precision a signal which is comparable or lower than the foreground contamination in presence of noise is remarkable. Once again, the observed performance is made possible by the large number of pixels in the map, as well as the high level of statistical independence between background and foreground emission. These two facts bring the algorithm close to an ideal environment, ensuring the convergence very close to the correct answer, with a precision represented by the

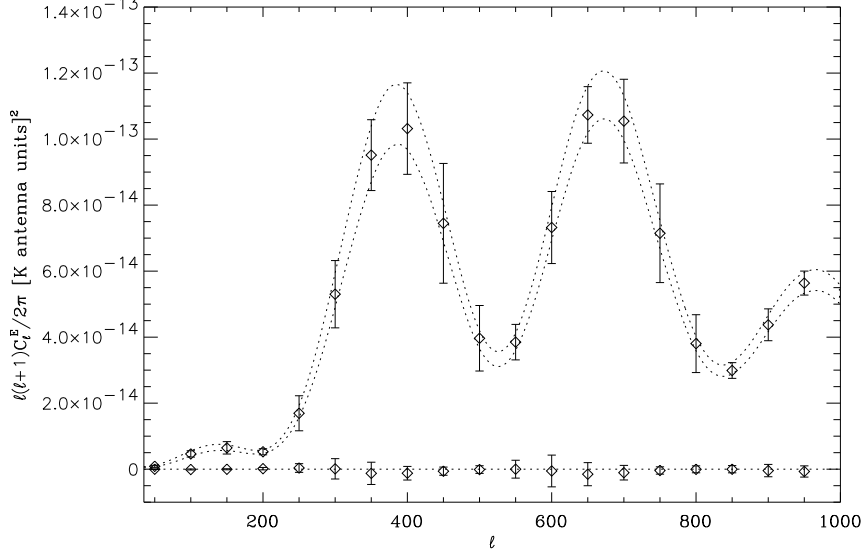


Figure 5. Pseudo-power spectra of the reconstructed \tilde{C}_l^E modes of the CMB in the 40, 90 GHz frequency combination, in the $S/N = 2$ case. The region between the dotted lines is the theoretical CMB signal $\pm\sigma$ cosmic and noise variance at 40 GHz on the sky area considered. At the bottom we show the average and standard deviation of the residuals on each realization.

errors shown in the figures.

A second, most interesting aspect to be noted is that we detect the error due to the separation process; that is clearly visible in all the figures as the excess in the error bars with respect to what predicted by cosmic variance and noise. The error from component separation is comparable or smaller, to the sample variance of the simulated templates. The error of the separation is either due to the randomness of the noise realizations on one hand and the fact that, for a single realization, background and foreground may not be completely independent. The latter factor can be a source of the extra randomness in the ICA performance thus contributing to the total error.

Although in this work we are mainly interested in the extraction of the CMB B modes from the data, it is interesting also to look at the foreground recovery. In figure 9 we plot the reconstructed pseudo power spectra of the separated synchrotron compared with the original ones, reported with dotted lines. In this case the LIGHTICA is able to properly reconstruct the polarized signals of the foreground with good precision. On the other hand, the dust reconstruction fails, as it comes out heavily contaminated by the CMB, and with wrong normalization. This manifests that the separation with dust is more problematic, as it may be also noted by looking at figure 8, which shows excess power in the recovered spectra and residuals with respect to the input ones, and which is mostly concentrated at low multipoles where the dust spectrum is highest, see also figure 11. This occurrence should not be interpreted in terms of the different pattern of the foreground emission for dust and synchrotron, but in terms of the relative weight of it with respect to the background emission, as already noticed in earlier works (Maino et al. 2002; Baccigalupi et al. 2004). Due to the difference in the frequency scalings in the bands considered, in the 40, 90 GHz case the foreground and background signals are closer in amplitude with respect to the higher frequency combination; thus, at 150 GHz the CMB dominates over the dust while at 350 GHz the CMB emission is negligible. Indeed, this bias disappears if the foreground amplitude is raised by a factor of a few as we see next, and consequently the dust template can be better reconstructed.

Finally, note that our Monte Carlo analysis does not include varying the foreground template, a factor should be accounted for as well in order to quantify the error in the separation process in a comprehensive way. However, the modest knowledge of the foreground emissions as it is available at the present does not allow to estimate their statistics to a level high enough to vary their template in the Monte Carlo.

4.3 Varying noise, foreground amplitudes and analyzed area

We perform here a first study of a dependence of the results on some of the key simulation parameters. Specifically, we vary noise amplitude, foreground fluctuation amplitude, and extension of the sky area considered. We explore the corresponding parameter space by moving along the multiple “directions” within its volume and use the results to set constraints on the applicability of the LIGHTICA approach given the assumed foreground pattern, however, still in systematic free cases.

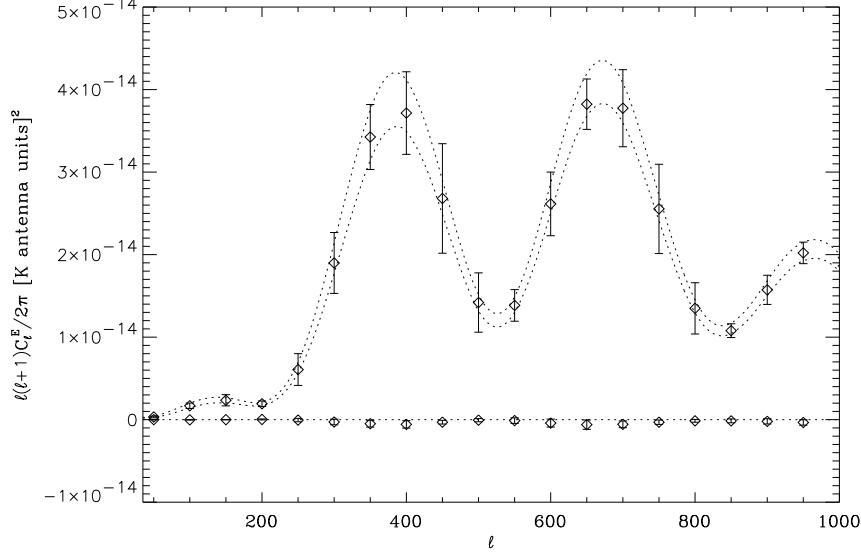


Figure 6. Pseudo-power spectra of the reconstructed \tilde{C}_l^E modes of the CMB in the 150, 350 GHz frequency combination, in the $S/N = 2$ case. The region between the dotted lines is the theoretical CMB signal $\pm\sigma$ cosmic and noise variance at 150 GHz on the sky area considered. At the bottom we show the average and standard deviation of the residuals on each realization.

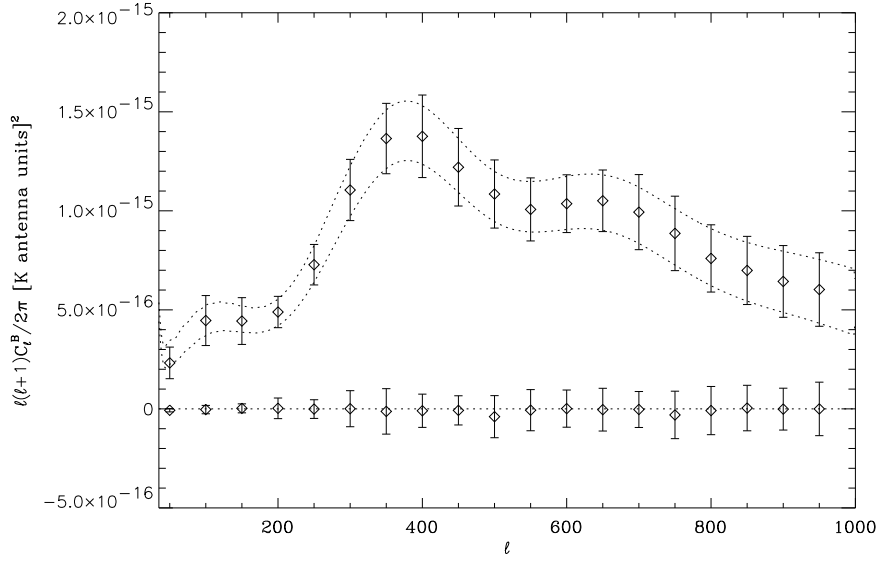


Figure 7. Pseudo-power spectra of the reconstructed \tilde{C}_l^B modes of the CMB in the 40, 90 GHz frequency combination, in the $S/N = 2$ case. The region between the dotted lines is the theoretical CMB signal $\pm\sigma$ cosmic and noise variance at 40 GHz on the sky area considered. At the bottom we show the average and standard deviation of the residuals on each realization.

In order to quantify the error introduced by the algorithm with respect to the one due to the cosmic variance and noise, and focusing on the B mode reconstruction, we introduce the quantities

$$d_l = \frac{\Delta \tilde{C}_l^{rec.}}{\Delta \tilde{C}_l^B}, \quad r_l = \left\langle \frac{\tilde{C}_l^{rec.} - \tilde{C}_l^B}{\tilde{C}_l^B} \right\rangle_{ICA}, \quad a_l = \left\langle \frac{|\tilde{C}_l^{rec.} - \tilde{C}_l^B|}{\tilde{C}_l^B} \right\rangle_{ICA}, \quad (11)$$

meaning of which we explain now. d_l is the ratio between the dispersion of the recovered spectra over 100 realizations and the quantity defined in (10). Generally we expect this quantity to be larger than 1, accounting for the error introduced by the separation itself: a number close to 1 means that the separation procedure introduces an error which is negligible with

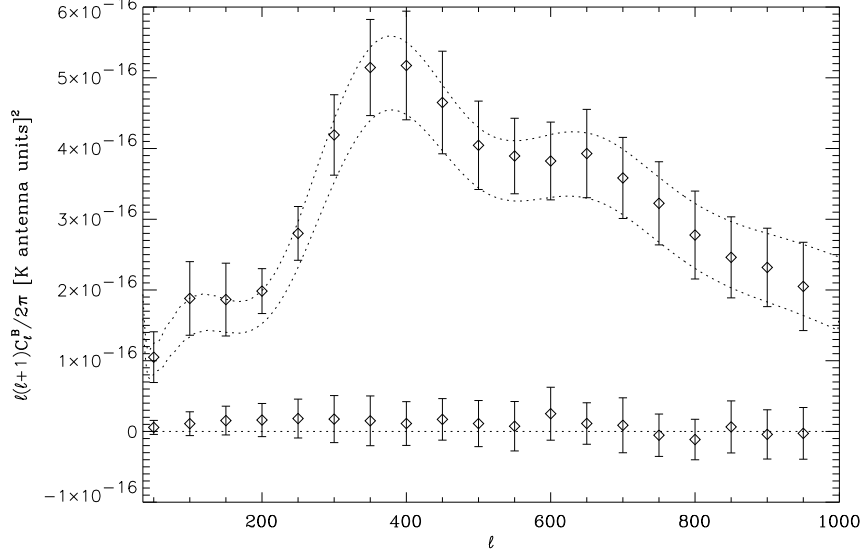


Figure 8. Pseudo-power spectra of the reconstructed \tilde{C}_l^B modes of the CMB in the 150, 350 GHz frequency combination, in the $S/N = 2$ case. The region between the dotted lines is the theoretical CMB signal $\pm\sigma$ cosmic and noise variance at 150 GHz on the sky area considered. At the bottom we show the average and standard deviation of the residuals on each realization.

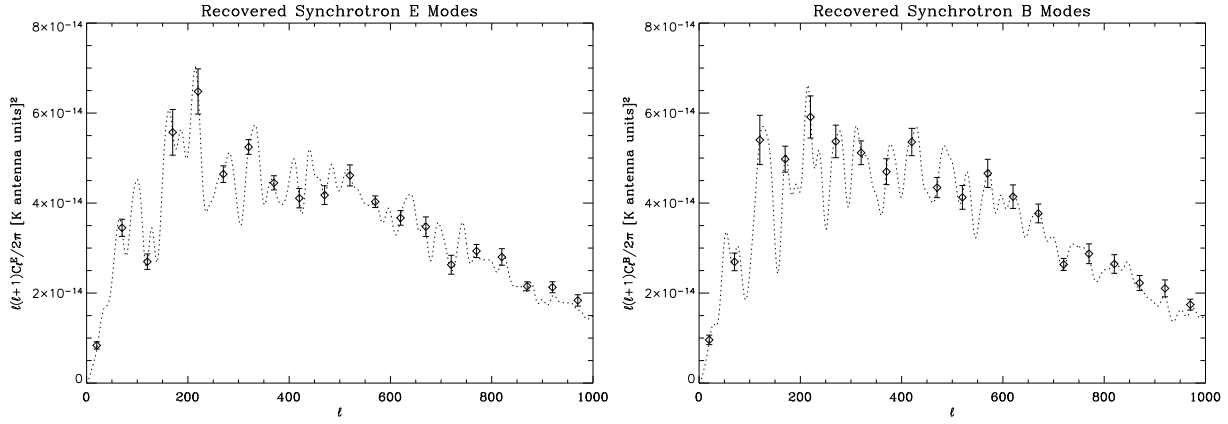


Figure 9. Pseudo-power spectra of the reconstructed \tilde{C}_l^E modes (left) and \tilde{C}_l^B (right) of synchrotron at 40 GHz in the $S/N = 2$ case. Dotted lines are the theoretical spectra.

respect to the input one; on the contrary, a value larger than 2 means that the separation error is dominating. d_l is a measure of the extra uncertainty introduced by the algorithm.

On the other hand, as we see in a moment, d_l may get closer to 1 when the noise is increased, leading to the apparent paradoxical conclusion that the LIGHTICA works better when more noise is considered. This is due to the fact that in some cases, the separation quality deterioration, caused by the increase of the noise level, proceeds at the slower rate than the noise level increase itself leading to a decrease in d_l . The r_l and a_l quantities are respectively the residual and the absolute residual of the recovered pseudo power spectra in the single separation, averaged over 100 realizations. These quantities give a measure of a bias of the reconstruction, and thus are expected to be close to zero. Note that part of the differences in the numerators of r_l and a_l comes from the instrumental noise; therefore, in a highly noisy configuration, their value can become large not because the separation fails, but because of the high noise itself.

Especially if checked together for each case, these quantities allow us to attempt to give a definition for a “successful” separation, which is when the LIGHTICA is able both to recover the CMB signal giving the value of d_l on one side and the values of r_l and a_l on the other close to, and less than unity, respectively. In tables 1, 2 and 3, we report the value of these quantities for some relevant multipoles as a function of the varying parameters.

We begin varying the noise with respect to the simulated dataset considered in the previous sub-section. We found out the

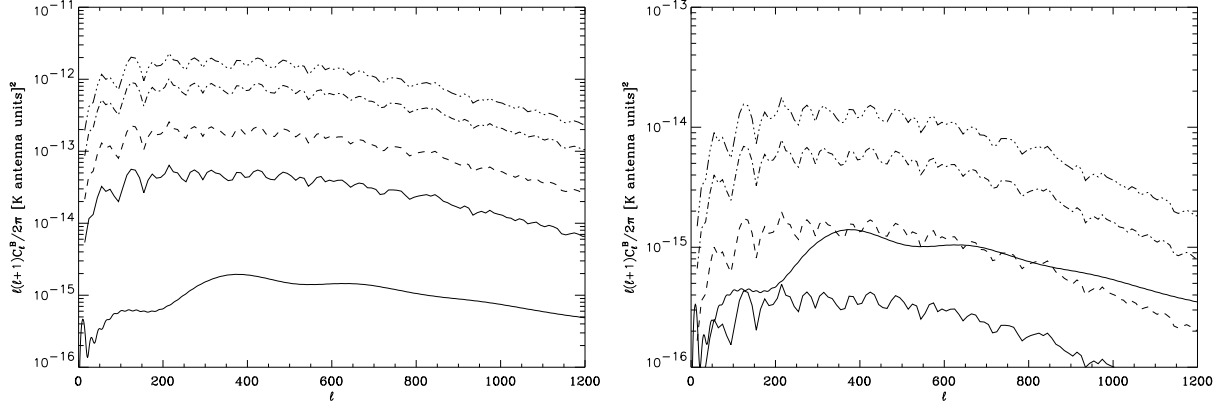


Figure 10. Pseudo-power spectra of the synchrotron B modes calculated for the sky region and with the amplitudes as considered in this work, at 40 (left) and 90 GHz (right). The different curves, with raising power, correspond to the foreground rms multiplied by 1, 2, 4, and 6, respectively. In each panel the solid smooth line represents the B modes of the CMB.

results to be quite stable up to $S/N = 1$. As it may be noted by looking at the first block of four rows in the tables, the algorithm performance, in terms of d_l , decreases mildly or remains constant, and decreases nearly linearly with the noise amplitude in terms of r_l and a_l . For of the noise larger than the signal, the code starts failing to reconstruct the signals, what at first shows as a residual foreground contamination persisting in the reconstructed B modes of the CMB, then as a failure to reach the convergence or to estimate a non-negative definite signal correlation matrix due to the large noise sample variance. The foreground variation is realized by keeping its mean over the considered area unchanged and increasing solely its rms by a factor 2, 4, and 6 for synchrotron, and 2, 4, 6 and 10 for dust. In figures 10 and 11 we report the foreground B modes at 40, 90 GHz and 150, 350 GHz, respectively, for the rms considered. For reference, we also plot the theoretical CMB pseudo-spectra. At 40 and 350 GHz, the contamination to the CMB is worse of course. Despite the high level of foreground fluctuations, the method exhibits again a remarkable stability or even improvement in the interval considered for this parameter, as it may be seen by looking at the second block of four rows in the tables; it starts failing only when the foreground rms is increased by a factor of about 6 for synchrotron, and by a factor of about 10 for dust. This can be interpreted as due to the fact that foreground recovery is indeed easier and more precise given a larger foreground amplitude. Indeed, for an ICA based component separation technique which utilizes the independence of the components to be recovered, the quality of the reconstruction of each of them depends on how well the other ones are extracted (Maino et al. 2002; Baccigalupi et al. 2004). The last row in each table shows the effect of the variation of the sky area considered, while all the other parameters are kept fixed. As expected, things get generally better after doubling the radius of the cut, but since at a resolution of about 10 arcminutes a patch with $\theta_C = 10^\circ$ has already a number of samples (pixels) large enough to faithfully represent the signal statistics, increasing θ_C doesn't improve the separation dramatically. However, a wider area represents a benefit concerning the possibility of detecting the B modes from primordial gravitational waves, as we discuss in section 5.

As a final remark, we notice that increasing the noise amplitude causes the reconstruction to be less accurate, in all cases when the dust is taken into account. This observation, anticipated in Section 4.2, is due to the fact that at 150 GHz, the dust emission is negligible with respect to CMB and noise. Indeed, as noticed in earlier works (Maino et al. 2002; Baccigalupi et al. 2004), the separation is more accurate when the signals are comparable in all frequency bands. This is supported by the fact that the performance improves or remains unaltered when the dust fluctuation amplitude is increased, while in the synchrotron case a clear degradation of the separation may be seen.

As a final test to evaluate the separation we study the recovered frequency scaling index $\alpha = \log[s(\nu_2)/s(\nu_1)]/\log(\nu_2/\nu_1)$ of the different output components s , computed through the ratios between column elements in the inverse of the separation matrix (Maino et al. 2002). In all the cases we studied, this quantity resulted to be close to the theoretical one, with dispersions $\Delta\alpha$ increasing roughly linearly with foreground amplitude and noise; an exception is still represented by the dust case, when the dust rms is increased: as explained above, increasing the dust rms induces an improvement in the reconstruction, which appears also in the recovery of α . The relative dispersion $\Delta\alpha/\alpha$, evaluated over the 100 Monte Carlo realizations both for CMB and foregrounds, is shown in table 4.

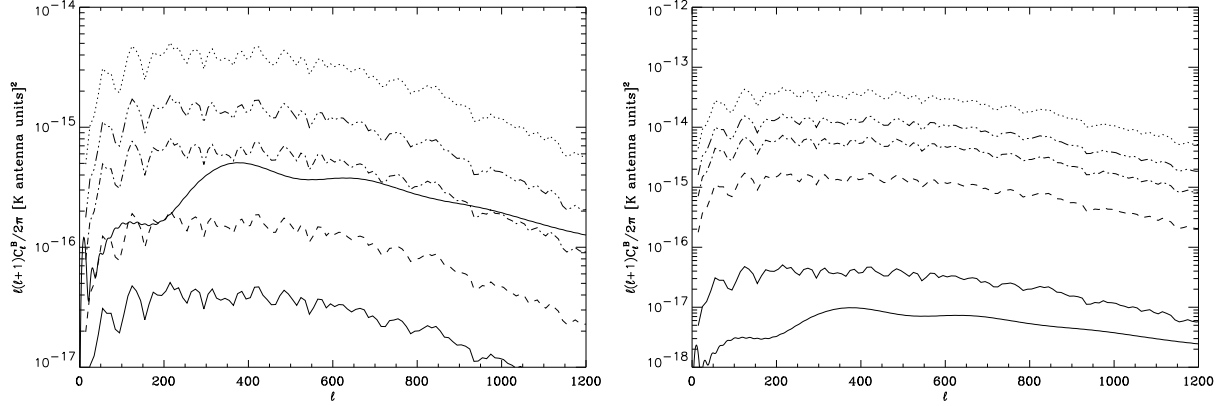


Figure 11. Pseudo-power spectra of the dust B modes calculated for the sky region and with the amplitudes as considered in this work, at 150 (left) and 350 GHz (right). The different curves, with raising power, correspond to the foreground rms multiplied by 1, 2, 4, 6 and 10, respectively. In each panel the solid smooth line represents the B modes of the CMB.

S/N	Fore. Ampl.	Cut Radius	$d_{l=100}$ Sync.	$d_{l=400}$ Sync.	$d_{l=950}$ Sync.	$d_{l=100}$ Dust	$d_{l=400}$ Dust	$d_{l=950}$ Dust
∞	1.00	10	1.16	1.69	1.31	2.08	1.99	1.74
2.00	1.00	10	1.44	1.55	1.18	1.81	1.56	1.31
1.50	1.00	10	1.38	1.42	1.07	2.24	1.56	1.31
1.00	1.00	10	1.88	1.72	1.38	3.39	1.56	1.21
2.00	2.00	10	1.60	1.70	1.33	1.66	1.64	1.34
2.00	4.00	10	1.62	2.03	1.58	1.63	1.69	1.33
2.00	6.00	10	1.78	2.39	1.81	1.51	1.69	1.32
2.00	10.00	10	-	-	-	2.00	2.04	1.50
2.00	1.00	20	1.28	1.53	1.03	1.75	1.41	1.24

Table 1. Relative extra uncertainty, d_l , evaluated for the reconstructed B mode power spectrum of the CMB. The results are given for three different values of the multipole l and for multiple choices of the sky and noise parameters as listed in the table.

S/N	Fore. Ampl.	Cut Radius	$r_{l=100}$ Sync.	$r_{l=400}$ Sync.	$r_{l=950}$ Sync.	$r_{l=100}$ Dust	$r_{l=400}$ Dust	$r_{l=950}$ Dust
∞	1.00	10	0.02	0.05	0.05	0.10	0.05	0.05
2.00	1.00	10	0.01	0.06	0.08	0.11	0.06	0.07
1.50	1.00	10	0.02	0.06	0.10	0.13	0.06	0.17
1.00	1.00	10	0.02	0.08	0.22	0.22	0.08	0.20
2.00	2.00	10	0.01	0.06	0.08	0.08	0.05	0.05
2.00	4.00	10	0.02	0.08	0.14	0.08	0.06	0.06
2.00	6.00	10	0.02	0.08	0.14	0.08	0.06	0.03
2.00	10.00	10	-	-	-	0.08	0.08	0.05
2.00	1.00	20	0.02	0.04	0.03	0.09	0.05	0.03

Table 2. Residuals of the CMB pseudo B modes recovered against synchrotron and dust, averaged over 100 realizations of noise and CMB.

S/N	Fore. Ampl.	Cut Radius	$a_{l=100}$ Sync.	$a_{l=400}$ Sync.	$a_{l=950}$ Sync.	$a_{l=100}$ Dust	$a_{l=400}$ Dust	$a_{l=950}$ Dust
∞	1.00	10	0.12	0.06	0.06	0.14	0.06	0.05
2.00	1.00	10	0.12	0.07	0.11	0.15	0.07	0.14
1.50	1.00	10	0.12	0.08	0.17	0.17	0.07	0.17
1.00	1.00	10	0.12	0.11	0.46	0.22	0.10	0.29
2.00	2.00	10	0.09	0.07	0.14	0.13	0.06	0.13
2.00	4.00	10	0.10	0.11	0.18	0.13	0.07	0.14
2.00	6.00	10	0.10	0.11	0.19	0.13	0.08	0.14
2.00	10.00	10	-	-	-	0.13	0.09	0.13
2.00	1.00	20	0.09	0.07	0.09	0.09	0.05	0.08

Table 3. Absolute value of residuals of the CMB pseudo B modes recovered against synchrotron and dust, averaged over 100 realizations of noise and CMB.

S/N	Fore. Ampl.	Cut Radius	CMB vs. Sync.	Synchrotron	CMB vs. Dust	Dust
∞	1.00	10	0.01	0.03	0.72	0.81
2.00	1.00	10	0.05	0.07	0.60	0.89
1.50	1.00	10	0.14	0.15	0.75	1.09
1.00	1.00	10	0.28	0.35	1.17	1.97
2.00	2.00	10	0.14	0.14	0.63	0.69
2.00	4.00	10	0.22	0.23	0.85	0.56
2.00	6.00	10	0.35	0.36	1.49	0.53
2.00	10.00	10	-	-	3.04	0.46
2.00	1.00	20	< 0.01	0.02	0.45	0.73
1.00	1.00	20	0.18	0.20	-	-

Table 4. Relative dispersions $\Delta\alpha/\alpha$ around the expected values of the frequency spectral indices, for both CMB and foregrounds.

5 MEASURING THE PRIMORDIAL TENSOR AMPLITUDE

As we stressed already, one of the most important goals of the forthcoming CMB polarization experiments is the measure of the ratio r between the primordial amplitudes of tensor and scalar cosmological perturbations, i.e. gravity waves and density fluctuations. The most relevant question in this context is how small that ratio can be in order to be detected when foregrounds are taken into account, and in particular what this minimal detectable value is when the CMB background is separated from the foregrounds with the technique considered here. As we stressed in section 2, the foreground simulations are still too uncertain to push the analysis toward a complete cosmological parameter estimation pipeline and address this question comprehensively. Nevertheless, given the importance of this topic, we present in this section some general though preliminary remarks and we illustrate them with some examples.

For our purpose here the most relevant result of the previous sections is the observation that the FASTICA-based separation yields errors which are comparable to those from cosmic variance and noise, for the model with $r = 0.1$. Therefore, in such a case, as far as these simulations are concerned, we should be able to detect the tensor contribution in the presence of foregrounds when the latter are treated with ICA, with a confidence close to the one achievable without foregrounds.

To illustrate this issue, we compare the pseudo B mode recovery in our fiducial model with $r = 0.1$ with one in which the tensors are absent, $r = 0$. We focus on the spectral region where primordial tensors are most relevant, e.g. $l \simeq 100$. Of course, as a result of the leakage of E modes into B due to the limited sky coverage, also in the latter case the amplitude

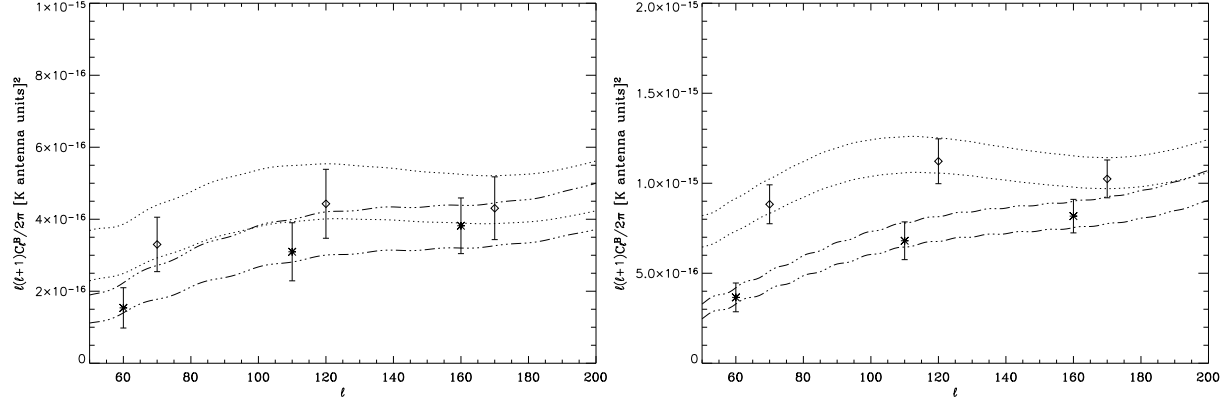


Figure 12. Comparison of the recovered pseudo- B modes in two different cosmological models with $r = 0$ (dashed-dotted lines and asterisks) and $r = 0.1$ (dotted lines and diamonds shifted by $\Delta l = 10$ for clarity), in the low frequency combination with $S/N = 2$. Left panel refers to $\theta_C = 10^\circ$, while right panel to $\theta_C = 20^\circ$. Regions between the lines are the dispersion coming from cosmic variance and noise.

of E modes on these scales also matters. We address this issue to some extent by considering the results for each value of r obtained for sky areas with different aperture. In figure 12 we plot the recovered pseudo B modes in these two cases, zooming on the relevant range of multipoles. Two different sizes for the sky cut are considered here; the left and right panel refer to $\theta_C = 10^\circ$ and $\theta_C = 20^\circ$, respectively. In both panels the higher amplitude spectrum represents the model with $r = 0.1$. As we quoted above, we see that in the entire interval, the separation error is comparable to the cosmic variance, in particular in the l -range, where the B modes from tensors have their main impact, i.e. $l \simeq 100$. The central role of the leakage from E modes is evident. When the area gets smaller and the pollution consequently larger, the detection of B modes becomes harder. Points on the plot are the pseudo B modes recovered by the code against the synchrotron template, in the case with $S/N = 2$, for both the models (asterisks for $r = 0$ and diamonds $r = 0.1$).

Looking at the left panel of the figure, it is clear that, even if the algorithm did not introduce any extra uncertainty, we could not make any claim on primordial B modes detection with sufficient confidence, mostly because the leakage is already too high for the 10 deg cut. The situation gets better for the $\theta_C = 20^\circ$ case (the right panel), where the two models seem to be distinguishable statistically by our method. For the latter case, more quantitative results are showed in table 5. To define whether or not the algorithm is able to distinguish between the two models, we compare the statistics of the recovered power spectra. In the second column, we report the percentage of recovered power spectra (for $r = 0$) that fall inside the 95% confidence region for $r = 0.1$ as calculated directly from the statistics of the recovered power spectra themselves. In this way, we obtain the probability for ICA to give a false detection of tensor contribution. Viceversa, the fourth column shows the probability to miss a true presence of primordial B modes, since it reports the percentage of recovered power spectra for $r = 0.1$ that fall inside the 95% confidence region for $r = 0$. Third and fifth column give the same probabilities but computed for simulated, CMB-only spectra and thus not requiring any further processing. These columns provide an idea of the best achievable levels.

We thus conclude that, given the available foreground simulations, FASTICA eliminates the foregrounds in the two cases of r we consider, with a precision sufficient to make them distinguishable even with the suboptimal pseudo-BB estimator. As already stressed above, this is due to the fact that the separation process induces an error comparable to those coming from cosmic variance and noise.

Further analysis on the recovering of the true B modes and, mostly important, on the minimum value of r that can be detected with this technique, could be performed (for problems relevant to this issue and what can be expected for the considered cases, see e.g. Lewis (2002, 2003) and reference therein). However they would not only go beyond the intended aim of this work, which is to show the capability of ICA in a situation close to what we expect for the forthcoming CMB polarization experiments, but could also prove to be misleading given the substantial uncertainties that still affect the foreground simulations and because of systematics in this simulation. We actually plan to address these issues in a future work, probably exploiting the new *pure* pseudo power spectrum estimator from Smith (2005), in a new, more realistic simulated environment.

	$\tilde{C}_{r=0}^{out}$ vs $\tilde{C}_{r=0.1}^{out}$	$\tilde{C}_{r=0}^{in}$ vs $\tilde{C}_{r=0.1}^{in}$	$\tilde{C}_{r=0.1}^{out}$ vs $\tilde{C}_{r=0}^{out}$	$\tilde{C}_{r=0.1}^{in}$ vs $\tilde{C}_{r=0}^{in}$
$\ell = 70$	0%	0%	0%	0%
$\ell = 120$	0%	0%	5%	2%
$\ell = 170$	50%	43%	53%	46%

Table 5. This table reports the capability of the algorithm to distinguish between the two models with and without the gravity wave content for the $\theta_C = 20^\circ$ case. The second column shows the probability (see text for more details) a spurious detection of the tensor contribution, while the fourth column shows the probability of a false non-detection. The other two columns report the same probabilities but derived in the ideal, CMB-only, foreground-free case.

6 DISCUSSION

In this work we discuss the performance of the component separation technique based on the Independent Component Analysis (ICA) as applied to the small patches of the polarized sky observed in the microwave band. We focus on the recovery of the Cosmic Microwave Background (CMB) signal out of the contamination due to the diffuse foreground emission from the Galaxy and perform a Monte Carlo analysis to estimate the resulting errors. These computations employ LIGHTICA – a newly developed parallel implementation of the FASTICA code (Hyvärinen 1999; Maino et al. 2002). The sky region considered here is and has been, the target of several CMB experiments due to its known low foreground emission in total intensity. Nevertheless, the current knowledge of the foreground emissions indicates that their contaminations to the CMB emission in polarization may be non-negligible in any region of the sky, and at any frequency considered, including sky areas which appear nearly free of the foregrounds in total intensity. This observation is particularly relevant for the component of the CMB signal due to the primordial gravitational waves and lensing mechanisms (B modes); the latter signal is extremely relevant in modern cosmology as it may demonstrate the existence of gravitational waves of cosmological origin, as well as reveal crucial clues about the structure formation in the universe.

The idea behind the ICA is based on the assumption that the background and foreground statistics are independent, requiring no other prior on the signals to recover, on their pattern or frequency scaling. All the available data and simulations on the Galactic foreground emission indicate that the CMB and Galactic emission are highly statistical independent; indeed, the CMB is known to have a statistics which is close to the Gaussianity, while the Galaxy is known to be highly non-Gaussian. This occurrence, together with the high level of detail in the present CMB data, reaching the arcminute scale, allow the ICA technique to recover the CMB pattern extremely close to the actual one.

We consider two sets of two frequency bands where the foreground contamination is given by the synchrotron and the thermal dust, respectively, and we assume a Gaussian and uniform noise distribution with amplitude comparable to the total CMB polarized emission. We quantify the quality of the reconstruction by comparing the input and output angular power spectra on the sky fraction which we consider (pseudo power spectra). Due to its parallelized structure, the LIGHTICA allows to evaluate the error in the separation process on each relevant angular scale, via Monte Carlo simulations sampling some of the most relevant degrees of freedom entering in the dataset simulation. We identify the error induced by the separation process on the CMB reconstruction and show that is comparable or lower than the uncertainty given by the instrumental noise and cosmic variance. We remark that in terms of pseudo- B modes, this is achieved in presence of a foreground contamination which may be several times stronger than the cosmological signal, which has been simulated accordingly to the current polarized foreground models. Then, we evaluate the stability of these results against variation of the noise and foreground fluctuation amplitude, as well as the sky area covered and the abundance of primordial gravitational waves. We find considerable intervals of these parameters where the results do not change substantially. In particular, the claim that the error induced by the reconstruction is of the order of the cosmic plus noise sample variance, remains true in all these cases. Moreover, the outputs exhibit a remarkable stability for a large foreground fluctuation amplitude, several times larger than predicted by the current foreground models; this may be due to a compensation between the degradation which would be induced by the large foreground signal, and the fact that the latter is better extracted as it gets larger over the noise. Then, we found that increasing the area covered yields an improvement of the separation performance, not too large since the smaller cut already contains enough statistical information to provide good convergence. By comparing the results with smaller and higher areas when the primordial tensor to scalar ratio is $r = 0.1$ and $r = 0$, we were able to check the benefit of having a larger area for measuring r , due to the weaker leakage from E modes. We were able to verify that for an area large as 20×20 squared degrees, the cases with $r=0.1$ and 0 are distinguishable even at the level of the suboptimal pseudo B mode power spectra at $l = 100$, after ICA has removed a foreground contamination which may be several times larger than the cosmological signal. We stress that this claim needs more investigation in the future due to the foreground uncertainties and absence of systematics, as we explain below.

We did not specialize our treatment for any specific experimental setup, but rather focused on a handful of important but quite general and basic parameters. This is because our aim is to show that if the foreground contamination to the

B modes of the CMB turns out to be consistent as the current foreground models predict, then an ICA based component separation may be required and adequate to achieve the detection of the cosmological signal. It is still premature to attempt a quantitative estimation of the ICA nominal performance taking into account the uncertainty in the foreground signal, in general or for a given experiment. Indeed, as we explain below the available information on the Galactic polarized signal is still too modest to assess properly its statistical distribution. Nevertheless, it is worthwhile to compare frequencies, angular resolution and noise amplitude of the planned and ongoing CMB polarization observations, with our assumptions. We thus note that the configuration at high frequencies, for angular resolution and noise amplitude, is close to the BOOMERanG case (Montroy et al. 2005). Our high frequency combinations are also close to those adopted by EBEx (Oxley et al. 2004) and QUAD (Bowden et al. 2004), while 40 and 90 GHz setup is adopted by QUIET. These two experiments have also an angular resolution close to what we assumed herein, however, given that they explicitly aim at the B mode detection, their nominal noise amplitude is markedly lower with respect to what we considered here and what was set to be comparable to the CMB rms in Q or U maps and hence to that of the E mode.

It is useful to recall here the limitations of the present analysis. First of all, a definitive assessment of the performance of ICA or any other component separation technique should come when the foregrounds simulations are put on a firmer ground. At the present the models are built upon observations in the radio or far infrared bands as well as the WMAP three year data (Page et al. 2006), used to constraint the polarization angle pattern, while the polarization fraction with respect to total intensity is often inferred from large scale data only. Moreover, the effects of extra-Galactic point sources were not considered here. The basic treatment of them in an experiment aiming at the detection of the diffuse signal is the identification and removal of the brightest ones, usually at 5σ from the rms of the diffuse signals plus noise; the remaining unresolved ones yield an angular power spectrum also rising approximately as l^2 . More sophisticated techniques involve the use of wavelets to identify and remove also fainter sources (Vielva et al. 2003), which have been proved so far promising for the identification and removal of all sources down to a flux comparable with the one from the diffuse signals plus noise. Actually, according to the latest models (Tucci et al. 2004), the angular power spectrum in B from extra-Galactic radio sources, where only the brightest have been removed, is actually comparable with the noise we consider in this work at 40 GHz, being subdominant at higher frequencies. An analogous situation might occur at 350 GHz, from the contribution to infrared sources if they possess an high polarization ratio, say one percent or more, although those are very poorly known. Our separation results were quite stable also for a lower signal to noise ratio, which seems to indicate that if the rms of the unresolved sources in the maps is estimated correctly, then the ICA should be relatively insensitive to them. This claim is certainly premature due to the foreground uncertainties, affecting extra-Galactic sources together with the diffuse Galactic signal, making difficult an accurate estimation of the contribution from unresolved sources to the noise, and possibly requiring a deeper source removal with appropriate techniques. Another important aspect concerns the simulation of the CMB itself. The latter is evaluated assuming a Gaussian statistics, while the lensing distortion, which is responsible for a large portion of the signal in the B polarization modes, causes a non-Gaussian distortion. The latter is caused by the correlation of different cosmological scales induced by the lensing mechanism. Numerical machineries to lens a Gaussian CMB realization are becoming available, see Lewis (2005). Although this issue is still under investigation, in particular for the effect on pseudo- C_l s on a limited patch of the sky, it has to be considered in future works on the present subject; in a MonteCarlo pipeline for evaluating the errors of the CMB reconstruction in the present and other cases, one should use the proper CMB templates, i.e. obtained by varying the primordial Gaussian realization as well as its non-Gaussian lensing distortion.

It is also important to stress the ICA fundamental hypotheses and limitations at the present level of the code architecture. Together with the statistical independence, which is likely to be very well verified for the CMB and the Galaxy, a fundamental limitation is represented by the assumption that the signals scale rigidly in frequency, which means that the spectral index is spatially independent. This is not verified on the whole sky, as both the energy distribution of free electrons, as well as the thermal dust temperature, exhibit fluctuations. On the other hand, so far there is no evidence that the synchrotron spectral index actually vary substantially on the angular scales considered in experiments observing a limited fraction of the sky, which is usually comparable to a percent of the sky. In addition, in the real space the ICA requires to work at the same angular resolution at all frequencies, which is not the case for most of the operating of planned observations. This makes necessary to work at the lowest resolution, or an approach in the harmonic space should be implemented. The ICA technique has also degrees of freedom which were not fully exploited yet. First, the neg-entropy approximation which is being used is still the original one, which was introduced in other context, with very different purposes from the present, cosmological applications. The question whether or not a more appropriate neg-entropy approximation exists for the problem at hand is still open. Moreover, the possibility to use priors on the mixing matrix and/or foregrounds should be taken into account, as it was done by Maino et al. (2003) for the first time. In polarization, where foregrounds are most uncertain, a possible constraint could come from the black-body frequency scaling for the CMB, which was not exploited so far.

Ultimately, all our results have been obtained in absence of instrumental systematics. The stability of the performance in these nominal conditions has to be quantified and verified in presence of the most important systematics effects, such as non-uniform and non-gaussian noise, beam asymmetry, etc.

However, we believe that the excellent performance shown here justifies the interest and effort toward the implementation

of techniques based on the Independent Component Analysis in real experimental conditions. Even if only a fraction of their capability remains in a real experiment application, that might be crucial in order to measure the actual pattern of the B-mode component of the CMB polarized emission.

ACKNOWLEDGMENTS

Carlo Baccigalupi is grateful to George F. Smoot for several useful discussions. Some of the results in this paper have been derived using the Hierarchical Equal Area Latitude Pixelization of the sphere (HEALPix, Górski et al. (2005)). The theoretical power spectra were calculated using the CMBFAST software by Seljak, Zaldarriaga (1996). We acknowledge the use of National Energy Research Scientific Computing Center computing resources. This research was supported in part by the NASA LTSA grant NNG04GC90G.

REFERENCES

- Amari S., Chichocki A., 1998, *Proc. IEEE* 86, 2026
- Baccigalupi C. et al., 2000, *MNRAS* , 318, 769
- Baccigalupi C. et al., 2001, *Astron. & Astrophys.* 372, 8
- Baccigalupi C., 2003, *New Astron. Rev.* 47, 1127
- Baccigalupi C. et al., 2004, *MNRAS* 355, 5570
- Bennett C.L. et al., 2003, *Astrophys. J. Suppl.* 148, 97
- Benoit A. et al., 2004, *Astron. & Astrophys.* 424, 571
- Carretti E., Bernardi G., Sault R.J., Cortiglioni S., Poppi S., 2005 *MNRAS* in press, preprint [astro-ph/0412598](http://arxiv.org/abs/astro-ph/0412598)
- Bouchet F.R., Prunet S., Sethi S.K., 1999, *MNRAS* , 302, 663
- Bowden M. et al., 2004, *MNRAS* 349, 321
- Brouw W.N., Spoelstra T.A.T., 1976, *Astron. & Astrophys. Suppl.* 26, 129
- Chon, G., Challinor A., Prunet S., Hivon E. Szapudi I., 2004, *MNRAS* 350, 914
- Delabrouille J., Cardoso J.F., Patanchon G., 2003, *MNRAS* 346, 1089
- Donzelli S. et al., 2005, *MNRAS* in press, preprint arxiv.org/abs/astro-ph/0507267
- Duncan A.R., Reich P., Reich W., Fürst E., 1999, *Astron. & Astrophys.* 350, 447
- Finkbeiner D.P., Davis M., Schlegel D.J. 1999, *Astrophys. J.* 524, 867
- Gabor D., 1946, *J. Inst. Elect. Eng.* 93, 420
- Giardino G. et al., 2002, *Astron. & Astrophys.* 387, 82
- Górski K.M. et al., 2005, *Astrophys. J.* 633, 759
- Hansen F.K., Górski K.M., Hivon E., 2002, *MNRAS* 336, 1304
- Haslam C.G.T., Stoffel H., Salter C.J., Wilson W.E., 1982, *Astron. & Astrophys. Suppl.* 47, 1
- Hyvärinen A., 1999, *IEEE Signal Processing Lett.* 6, 145
- Hobson M.P., Jones A.W., Lasenby A.N., Bouchet F., 1998, *MNRAS* 300, 1
- Jones T.J., Klebe K., Dickey J.M., 1992, *Astrophys. J.* 389, 602
- Kamionkowski M., Kosowsky A., Stebbins A., 1997, *Phys. Rev. D* 55, 7368
- Kogut A. et al., 2003, *Astrophys. J. Suppl.* 148, 161
- Kovac J. et al., 2002, *Nature* 420, 772
- Lewis A., Challinor A., Turok N., 2002, *Phys. Rev. D* 65, 023505
- Lewis A., 2003, *Phys. Rev. D* 68, 083509
- Lewis A., 2005, *Phys. Rev. D* 71, 083008
- Maino D. et al., 2002, *MNRAS* 334, 53
- Maino D., Banday A.J., Baccigalupi C., Perrotta F., Górski K., 2003, *MNRAS* 344, 544
- Mesa D. et al., 2002, *Astron. & Astrophys.* 396, 463
- Montroy T. et al., 2005, submitted to *Astrophys. J.* , preprint available at arxiv.org/abs/astro-ph/0507514
- Oxley P. et al., 2004, *Earth Observing Systems IX*. Edited by William L. Barnes and James J. Butler, Proceedings of the SPIE, 5543, 320
- Page L. et al., 2006, preprint arxiv.org/abs/astro-ph/0603450
- Prunet S., Sethi S.K., Bouchet F.R., Miville-Deschenes M.A., 1998, *Astron. & Astrophys.* 339, 187
- Readhead A.C.S., 2004, *Science* 306, 836
- Sazonov S.Y., Sunyaev R.A., 1999, *MNRAS* 310, 76
- Seljak U., Hirata C.M., 2004, *Phys. Rev. D* 69, 043005
- Seljak U., Zaldarriaga M., 1996, *Astrophys. J.* 469, 437

- Smith K.M., Hu W., Kaplinghat M., 2004, *Phys. Rev. D* 70, 043002
- Smith K.M., 2005, preprint arxiv.org/abs/astro-ph/0511629
- Spergel D.N. et al., 2003, *Astrophys. J. Suppl.* 148, 175
- Stolyarov V., Hobson M.P., Ashdown M.A.J., Lasenby A.N., 2002, *MNRAS* 336, 97
- Tegmark M., 1997, *Phys. Rev. D* 55, 5895
- Tegmark M., Efstathiou G., 1996, *MNRAS* 281, 1297
- Tucci M., et al., 2002, *Astrophys. J.* 579, 607
- Tucci M., Martínez-González E., Toffolatti L., Gonzalez-Nuevo J., De Zotti G., 2004, *MNRAS* 349, 1267
- Tucci M., Martínez-González E., Vielva, P., Delabrouille, J., 2005, *MNRAS* 360, 935
- Uyaniker B., Fürst E., Reich W., Reich P., Wielebinski R., 1999, *Astron. & Astrophys. Suppl.* 138, 31
- Vielva P., Martínez-González E., Gallegos J.E., Toffolatti L., Sanz D., 2003, *MNRAS* 344, 89
- Zaldarriaga M., 2001, *Phys. Rev. D* 64, 103001
- Zaldarriaga M., Seljak U., 1997, *Phys. Rev. D* 55, 1830
- Zaldarriaga M., Seljak U., 1998, *Phys. Rev. D* 58, 023003